HHS Public Access

Author manuscript

Arterioscler Thromb Vasc Biol. Author manuscript; available in PMC 2023 March 08.

Published in final edited form as:

Arterioscler Thromb Vasc Biol. 2022 October ; 42(10): 1244–1253. doi:10.1161/ATVBAHA.122.317686.

The Nonproteolytic Intracellular Domain of Membrane-Type 1 Matrix Metalloproteinase Coordinately Modulates Abdominal Aortic Aneurysm and Atherosclerosis in Mice—Brief Report

Michele Silvestro,
Division of Vascular and Endovascular Surgery, Department of Surgery, New York University Langone Medical Center, New York.

Cristobal F. Rivera,
Division of Vascular and Endovascular Surgery, Department of Surgery, New York University Langone Medical Center, New York.

Dornazsadat Alebrahim,
Division of Vascular and Endovascular Surgery, Department of Surgery, New York University Langone Medical Center, New York.

John Vlahos,
Division of Vascular and Endovascular Surgery, Department of Surgery, New York University Langone Medical Center, New York.

Muhammad Yogi Pratama,
Division of Vascular and Endovascular Surgery, Department of Surgery, New York University Langone Medical Center, New York.

Cuijie Lu,
Division of Rheumatology, Department of Medicine, New York University Langone Medical Center, New York.

Claudia Tang,
Division of Vascular and Endovascular Surgery, Department of Surgery, New York University Langone Medical Center, New York.

Zander Harpel,
Division of Vascular and Endovascular Surgery, Department of Surgery, New York University Langone Medical Center, New York.

Rayan Sleiman Tellaoui,

Correspondence to: Bhama Ramkhelawon, Division of Vascular and Endovascular Surgery, Department of Surgery, New York University Langone Medical Center, New York, NY. bhama.ramkhelawon@nyulangone.org.

Disclosures
None.

Supplemental Material
Major Resources Table

Supplemental Material is available at https://www.ahajournals.org/doi/suppl/10.1161/ATVBAHA.122.317686.

Division of Vascular and Endovascular Surgery, Department of Surgery, New York University Langone Medical Center, New York.

Ariadne L. Zias,
Division of Vascular and Endovascular Surgery, Department of Surgery, New York University Langone Medical Center, New York.

Delphina J. Maldonado,
Division of Vascular and Endovascular Surgery, Department of Surgery, New York University Langone Medical Center, New York.

Devon Byrd,
Division of Vascular and Endovascular Surgery, Department of Surgery, New York University Langone Medical Center, New York.

Mukundan Attur,
Division of Rheumatology, Department of Medicine, New York University Langone Medical Center, New York.

Paolo Mignatti,
Division of Rheumatology, Department of Medicine, New York University Langone Medical Center, New York.

Department of Cell Biology, New York University Langone Medical Center, New York.

Bhama Ramkhelawon
Division of Vascular and Endovascular Surgery, Department of Surgery, New York University Langone Medical Center, New York.

Department of Cell Biology, New York University Langone Medical Center, New York.

Abstract

BACKGROUND: MT1-MMP (membrane-type 1 matrix metalloproteinase, MMP-14) is a transmembrane-anchored protein with an extracellular proteinase domain and a cytoplasmic tail devoid of proteolytic functions but capable of mediating intracellular signaling that regulates tissue homeostasis. MT1-MMP extracellular proteolytic activity has been shown to regulate pathological remodeling in aortic aneurysm and atherosclerosis. However, the role of the nonproteolytic intracellular domain of MT1-MMP in vascular remodeling in abdominal aortic aneurysms (AAA) is unknown.

METHODS: We generated a mutant mouse that harbors a point mutation (Y573D) in the MT1-MMP cytoplasmic domain that abrogates the MT1-MMP signaling function without affecting its proteolytic activity. These mice and their control wild-type littermates were subjected to experimental AAA modeled by angiotensin II infusion combined with PCSK9 (proprotein convertase subtilisin/kexin type 9) overexpression and high-cholesterol feeding.

RESULTS: The mutant mice developed more severe AAA than the control mice, with concomitant generation of intraaneurysmal atherosclerotic lesions and dramatically increased macrophage infiltration and elastin degradation. Aortic lesion-associated and bone marrow–derived macrophages from the mutant mice exhibited an enhanced inflammatory state and

expressed elevated levels of proinflammatory Netrin-1, a protein previously demonstrated to promote both atherosclerosis and AAA.

CONCLUSIONS: Our findings show that the cytoplasmic domain of MT1-MMP safeguards from AAA and atherosclerotic plaque development through a proteolysis-independent signaling mechanism associated with Netrin-1 expression. This unexpected function of MT1-MMP unveils a novel mechanism of synchronous onset of AAA and atherogenesis and highlights its importance in the control of vascular wall homeostasis.

Graphical Abstract

A graphic abstract is available for this article.

Keywords

angiotensin; aortic aneurysm; abdominal; atherosclerosis; macrophages; matrix metalloproteinase 14; matrix metalloproteinases; Netrin-1

Abdominal aortic aneurysm (AAA), a disease characterized by degeneration of the aortic wall, manifests as a dilation of the abdominal aorta of at least 1.5× the baseline diameter.[1] In spite of significant variation in progression and severity of the disease,[1] most patients remain asymptomatic until aneurysmal rupture. Following rupture, mortality is as high as 90%, rendering AAA a silent killer. The only treatment for AAA relies on surgical intervention, including open or endovascular procedure options, depending on patient anatomy. No noninvasive treatments targeting the early stages of disease are currently available. The demand for pharmacological approaches highlights the need for a better understanding of the biological mechanisms that drive AAA generation and progression.

The pathological remodeling of the extracellular matrix of the aortic wall is a critical driver of AAA development.[2–5] It is now well established that extracellular matrix degradation is primarily driven by members of the MMP (matrix metalloproteinase) family of proteolytic enzymes. Several MMPs, including MMP-2, MMP-9, and MMP-14 MT1-MMP (membrane-type 1 matrix metalloproteinase), have been associated with AAA severity in human studies.[6] Genetic and pharmacological approaches to mitigate MMP proteolytic activity protect against AAA development in several murine models.[2] However, although most of these studies have provided critical insights into the role of MMPs in promoting AAA, pharmacological approaches using MMP-specific proteinase inhibitors have failed to block AAA progression.[7] These results indicate that nonproteolytic function of MMPs could also intervene in the pathogenesis of AAA.

MT1-MMP, also known as MMP-14, a transmembrane proteinase with an extracellular proteolytic domain and a small cytoplasmic tail,[8–10] plays a central role in AAA formation by mediating macrophage-driven degradation of the aortic wall's elastic fibers.[11] Conversely, MT1-MMP inhibits atherosclerosis progression in ApoE knockout mice by inhibiting vascular smooth muscle cell proliferation.[12] These functions of MT1-MMP have been ascribed to its extracellular proteolytic activity. However, MT1-MMP has also been shown to possess a proteolysis-independent function mediated by its cytoplasmic tail, through which it activates the rat sarcoma oncogene-derived GTPase, also known as

p21 (Ras)-ERK1/2 (extracellular signal-regulated kinases 1 and 2, also known as p44/42) and AKT (serine/threonine kinase, also known as PKB [protein kinase B]) signaling pathways.[13,14] Substitution of the unique tyrosine in the cytoplasmic domain (Y573D) blocks this effect without affecting the proteolytic activity of MT1-MMP.[15] Adult mice harboring this mutation show altered bone, cartilage, and adipose tissue homeostasis as a result of impaired differentiation of bone marrow mesenchymal stem cells. These findings prompted us to investigate the potential role of the nonproteolytic signaling function of MT1-MMP in the control of vascular wall homeostasis.

Here, we report that expression of the signaling-defective MT1-MMP Y573D mutant in mice aggravates AAA development with concomitant intralesional atherosclerotic plaque formation. Notably, we identified that the downstream signaling mediated by MT1-MMP Y573D is associated with the expression of proatherogenic and proaneurysmal protein Netrin-1. These findings show that MT1-MMP intracellular signaling curbs the concomitant onset of AAA and atherosclerotic plaque development, an important novel function of MT1-MMP in vascular remodeling.

MATERIALS AND METHODS

Data Availability

Data, analytic methods, and study materials are available from the corresponding author upon reasonable request.

Mice

The generation and characterization of the phenotype of the MT1-MMP Y573D mouse has been described.[15] Three-month-old male homozygous mutants *Mmp14*$^{Y573D/Y573D}$ (YD) and wild-type *Mmp14*$^{wt/wt}$ (wt) littermates were used in these experiments.

As noted by the *Arteriosclerosis, Thrombosis, and Vascular Biology* Council statement,[16] "The low incidence of experimental AAA in females provides a challenge for studies in which interventions reduce the disease. Based on calculations of statistical power, it is likely that very large numbers of females will be needed to complete the studies. Hence, this provides a rationale for a restriction of studies to only male." Based on those recommendations and given the limited extent of this brief report study, we limited our experiments to male mice.

AAA Induction in Mice

Procedures described[17] by us and others were used to induce AAA in mice. Briefly, 12-week-old male mice and wild-type littermates were implanted with Alzet osmotic pumps (no. 2004; Durect Corporation) subcutaneously for a continuous 28-day delivery of PBS (control) or angiotensin II (H- 1705; Bachem) at 1 μg/kg per minute AAA was induced by increasing their cholesterol through intraperitoneal injection of adeno-associated viral vector (AAV) overexpressing PCSK9 (proprotein convertase subtilisin/kexin type 9) concomitant with Western diet (21% [wt/wt] fat, 0.3% cholesterol; Research Diets) feeding for 2 weeks before osmotic pump implantation. Mice developed AAA when maintained on Western

diet throughout the angiotensin II perfusion as described.[18] Upon euthanization, blood was collected by cardiac puncture. Plasma cholesterol was measured with an enzymatic assay (99902601, Fujifilm Wako Diagnostics). The CODA mouse tail-cuff high throughput system was used to measure blood pressure as per manufacturer's instruction (Kent Scientific Corporation). AAA severity was evaluated at euthanization based on gross morphological aortic alterations as per guidelines.[19] Aortas without dilation or sign of disease were scored as stage 0. Dilated aortas and aortas presenting a bulging without thrombus were scored as stages I and II, respectively. Bulbous aortas with visible thrombus were scored as stage III. In the case of death before experimental procedure completion, a necropsy would have been performed to assess the cause of death; rupture would have been characterized by the presence of an intraperitoneal hemorrhage and graded stage IV.

Doppler Ultrasound Imaging

Aortic diameter and Pulse Wave Velocity were assessed weekly using a Vevo 2100 ultrasound imaging platform (FUJIFILM VisualSonics).[20] Mice were anesthetized using 2% isoflurane inhalation, placed in a supine position and the abdominal region was shaved and coated with aquasonic ultrasound transmission gel (NC9861677, Parker Laboratories) before positioning the acquisition probe. Heart rate and basal temperature were monitored throughout the ultrasound imaging procedure. Color mode ultrasound was used to visualize the pararenal aorta. M-mode imaging was used to measure the suprarenal aortic diameter. Measurements were analyzed by a blinded observer.

Real-Time Quantitative Polymerase Chain Reaction

Aortic tissue samples were lysed in TRIzol (15596026, Ambion, Life Technologies) and RNA was extracted by a Directzol RNA MiniPrep Kit (R2052, Zymo Research). Following reverse transcription using a cDNA Synthesis Kit (1708890, Bio-Rad), quantitative real-time polymerase chain reaction (PCR) was performed with KAPA SYBR FAST quantitative PCR Kits (KK4602, KAPA Biosystems) using a QuantStudio 3 Real-Time PCR System (Applied Biosystems). The primer sequences used were:

28S: 5′-TGGGAATGCAGCCCAAG-*3′* and *5′*-CCTTACGGTACTTGTTGACTATCG-*3′*

Cd4: *5′*-TCCTTCCCACTCAACTTTGC-*3′* and *5′*-AAGCGAGACCTGGGGTATCT-*3′*

Cd8: *5′*-GCTCAGTCATCAGCAACT CG-*3′* and *5′*-ATCACAGGCGAAGTCCAATC-*3′*

Cd68: *5′*-TGTCTGATCTTGCTAGGACCG-*3′* and *5′*-GAGAGTAACGGCCTTTTTGTGA-*3′*

Mmp2: *5′*-CAAGTTCCCCGGCGATGTC-*3′* and *5′*-TTCTGGTCAAGGTCACCTGTC-*3′*

Mmp3: *5′*-GTCCCTCTATGGAACTCCCAC-*3′* and *5′*-AGTCCTGAGAGATTTGCGCC-*3′*

Mmp12: *5′*-GAGTCCAGCCACCAACATTAC-*3′* and *5′*-GCGAAGTGGGTCAAAGACAG-*3′*

Timp1: *5′*-GCAACTCGGACCTGGTCATAA-*3′* and *5′*-CGGCCCGTGATGAGAAACT-*3′*

Timp2: *5′*-TCAGAGCCAAAGCAGTGAGC-*3′* and *5′*-GCCGTGTAGATAAACTCGATGTC-*3′*

Timp3: *5′*-CTTCTGCAACTCCGACATCGT-*3′* and *5′*-GGGGCATCTTACTGAAGCCTC-*3′*

Ntn1: 5′-CAGCCTGATCCTTGCTCGG-*3′* and *5′*-GCGGG TTATTGAGGTCGGTG-*3′*

Tnfa: *5′*-GGTGCCTATGTCTCAGCCTCTT-*3′* and *5′*-GCCATAGAACTGATGAGAGGGAG-*3′*

Nos2: *5'*-GTTCTCAGCCCAACAATACAAGA-*3′* and *5′*-GTGGACGGGTCGATGTCAC-*3′*

Mrc1: *5′*-CTCTGTTCAGCTATTGGACGC-*3′* and *5′*-CGGAATTTCTGGGATTCAGCTTC-*3′*

Il1b: 5′-TGTGAATGCCACCTTTTGACA-3′ and 5′- GGT CAAAGGTTTGGAAGCAG-3′

Il6: 5′-CCGGAGAGGAGACTTCACAG-3′ and 5′- GGAAATTGGGGTAGGAAGGA-3′

Fold change differences were calculated after normalization to *28S* by the comparative cycle method ($2^{-\Delta\Delta Ct}$).

Cell Culture

For bone marrow–derived macrophage (BMDM) preparation, homozygous mutant YD or wt mice femurs and tibias were collected; the bone marrow was flushed and cells were cultured for 7 days in DMEM (MT10013CV, Fisher Scientific) supplemented with 10% Fetal Bovine Serum (FBS; 10082147, Life Technologies), 1% penicillin-streptomycin (30-002-CI, Corning), and 20% L-929 cell-conditioned medium. After differentiation, BMDM were polarized with ultrapure lipopolysaccharide (100 ng/mL; tlrl-3pelps; Invivogen) and recombinant IFN (interferon) γ (G3694, Life Span technology, 50 ng/mL) for M1 differentiation and with recombinant IL (interleukin)-4 (404-ML-010, R&D Systems, 20 ng/mL) for M2 activation. After 24 hours, cells were collected for RNA isolation and real-time PCR analysis. For TIMP (tissue inhibitor of metalloproteinases)-2 stimulation experiments, wt or YD BMDM were starved in DMEM supplemented with 2% FBS for 16 hours and stimulated with TIMP2 (410-02, 100 ng/mL; PeproTech) or vehicle for 15 minutes.

Immunofluorescence Staining and Microscopy Analysis

Seven micrometer thick sections of frozen aortic samples conserved in Optimal Cutting Temperature Compound (4585; Fisher Scientific) were fixed in 10% formalin buffer before immunostaining. Sections from paraffin-embedded samples were deparaffinized

and then processed for tissue rehydration and antigen retrieval using EDTA and Tween solution as described.[4] Cells were stained prior to fixation on Lab-Tek chamber slides (C7057, Millipore Sigma). Staining was performed by incubation with anti-CD68 (no. MCA1957, 5 μg/mL; Bio-rad), anti-Netrin-1 (ab39370, 500 ng/mL; Abcam), anti–Phospho-p44/42 MAPK (mitogen-activated protein kinase; Erk1/2; 9101s, 1 μg/mL; Cell Signaling), anti–α-smooth muscle actin (48938S, 250 ng/mL; Cell Signaling), Anti-SMAD1/3/5 (mothers against decapentaplegic homolog 1/3/5; phospho S423+S425; Ab51451, 5.5 μg/mL; Abcam), AlexaFluor 568 Phalloidin (A12380, 165 nmol/L; Invitrogen) and 4’,6-diamidino-2-phenylindole; D1306, 300 nM; Invitrogen) was used for visualization of nuclei. Images were acquired using a Zeiss LSM 710 confocal microscope (Carl Zeiss) through the Zeiss Efficient Navigation software (Carl Zeiss). Identical acquisition parameters were set to capture control and test samples.

Oil Red O, Elastin, and Collagen Staining

Frozen aortic cross-sections were stained with Oil Red O and counterstained with hematoxylin. Oil Red O–stained areas were quantified using Image J Software. Data are shown as percentage of Oil Red O–positive area relative to total intimal area. All plaques were analyzed from plaques within the same region at the site of maximum abdominal aortic diameter. For elastin staining, sections were stained using the Verhoeff-Van Gieson Elastin stain set (25089-1, Astral Diagnostics) according to the manufacturer’s instructions. Frozen sections were also stained with hematoxylin and eosin to observe atherosclerotic lesions. For collagen staining, sections were stained with Picrosirius Red (Polysciences, 24901–250) according to manufacturer’s instructions. Samples were examined with a microscope by a blinded experimenter. In addition to brightfield, acquisition under polarized light was used for Picrosirius red–stained sections. Quantification was performed using ImageJ software.

In Situ Zymography

Frozen abdominal aortic frozen samples embedded in Optimal Cutting Temperature Compound (4585, Fisher Scientific) were sectioned using a Cryostat to generate 7-μm-thick sections. Samples were incubated at 37 °C for 24 hours with a fluorogenic gelatin substrate (DQ gelatin; D12054, Invitrogen) dissolved in zymography buffer (25 μg/mL), as per manufacturer’s instructions. The proteolytic activity was measured as green fluorescence (530 nm). Autofluorescence of elastic laminae (461 nm) is shown in blue. Quantitative analysis of fluorescence intensity was obtained with ImageJ software.

Western Blotting

BMDM were lysed in RIPA (radioimmunoprecipitation assay) buffer (98065; Cell Signaling Technologies) supplemented with complete protease inhibitor cocktail (11697498001; Roche). Protein concentrations were determined using a colorimetric protein assay kit (5000001; Bio-Rad). Thirty micrograms of proteins were loaded onto a 10% mini-PROTEAN TGX gel (no. 456–8034, Bio-Rad) for SDS-PAGE and transferred to PVDF (polyvinylidene fluoride) membranes (no. BR20180416; Bio-Rad) using a Trans-Blot Turbo Transfer System (Bio-Rad). Primary anti–p44/42 MAPK (ERK 1/2; 4695, 84 ng/mL; Cell Signaling) and anti–Phospho-p44/42 MAPK (pERK 1/2 [phospho-ERK1/2]; 200 ng/mL, 9101s; Cell Signaling) antibodies were diluted in Tris Buffered Saline containing 1%

Casein (1610782; Bio-Rad), 0.1% Tween (J20605.AP; Thermo Scientific). Goat anti-rabbit IgG fluorescent antibody (StarBright Blue 700; 12004158, 1:2000 dilution; Bio-Rad) was incubated with the membranes for both of the antibodies. Anti-actin hFAB Rhodamine Antibody (12004163, 1:4000 dilution; Bio-Rad) as used as a loading control. Protein bands were imaged on a Bio-Rad ChemiDoc imaging system (Bio-Rad). Mean band intensities were normalized to control and quantified with ImageJ software.

Migration Assay

YD or wt BMDM seeded in the upper chamber of 24-mm transwell plates with 8.0-μm pores (3428; Costar) were challenged with recombinant CCL2 (C-C motif chemokine 2; 479-JE-050, 10 ng/mL; R&D Systems) or vehicle for 6 hours. Nonmigrated cells were scraped off before staining with Giemsa. Migrated cells were counted and imaged with an inverted microscope.

Statistical Analysis

Continuous variables are shown as means±SEM. Mann-Whitney tests were used to compare two groups of continuous data, as indicated. Comparisons among >2 independent groups were performed by Kruskal-Wallis test and Dunn multiple comparisons test or by mixed-effect model (REML [restricted maximum likelihood]) with Geisser-Greenhouse correction and Sidak's multiple comparisons test when appropriate. Statistical differences were calculated using Prism 9 software (GraphPad Software Inc, CA). $P<0.05$ were considered significant.

RESULTS

To study the effect of the MT1-MMP Y573D mutation on AAA development, mice homozygous for the mutation (*Mmp14*$^{Y573D/Y573D}$, YD) and control wild-type littermates (*Mmp14*$^{wt/wt}$, wt) were injected with an AAV overexpressing PCSK9 and fed a Western diet, as described.[4] Fourteen days later (time 0), all the mice received implantation of an osmotic pump delivering either Ang II (angiotensin II) or control PBS. AAA development was then characterized weekly by ultrasound imaging up to day 28, when the mice were euthanized (Figure 1A). Mice of both genotypes had comparable base levels of plasma cholesterol before PCSK9-AAV injection (day 14), and increased plasma cholesterol levels were confirmed 28 days after pump implantation (day 28) in all the mice, without significant differences between the 2 genotypes (Figure 1B). Quantitative ultrasound analysis at time 0 showed no significant difference in the diameter of the abdominal aorta between wt and YD mice (Figure 1C). However, following Ang II infusion, YD mice showed significantly more rapid dilation than wt mice, and on day 28 the aortic diameter was significantly larger in the mutant mice than in the wt controls (Figure 1C, right, and Figure 1D). Systolic arterial pressure at day 28 was comparable in mice of both genotypes (Figure 1E). Consistent with the increase in aortic diameter, color Doppler analysis showed dramatically increased blood flow turbulence in the aorta of YD versus wt mice (Figure 1F).

Macroscopic analysis of the aortas on day 28 (Figure 1G and 1H), when the animals were euthanized, showed comparable prevalence of AAA development in Ang II–treated mice of

both genotypes. However, over 50% of the YD mice had stage III AAA, whereas 100% of the wt mice had stage II lesions. This finding indicated that YD mice also developed accelerated intraaneurysmal lesions following only 6 weeks of Western diet feeding and on an *ApoE*$^{+/+}$ background.

Consistent with the macroscopic findings, microscopic analysis (Figure 1I) showed a dramatically decreased number of elastin fibers and increased degradation of the elastic laminae in YD mice relative to their control wt littermates.

As indicated by the different prevalence of stage III AAA, we found more advanced lesions in YD than in wt mice, which manifested with atherosclerotic features by microscopy. Consistent with the severity of the lesions observed in the aorta of YD mice transcriptomic characterization of the aortic tissue of wt and YD mice by quantitative PCR showed significant increases in the mRNA abundance of multiple MMPs and TIMPs, including *Mmp2* and *Mmp12*. *Timp1* and *2* mRNA levels also showed a significantly increased expression (Figure 1J). Notably, by in situ zymography, we observed increased proteolytic activity in aortic sections from mice challenged with Ang II, which was significantly increased in YD mice than in their control wt littermates (Figure 1K), in accordance with the more severe aortic pathology observed in YD mice.

Oil Red O staining of the aortic sections showed large atherosclerotic lesions associated with the AAAs of YD mice but not with those of wt mice (Figure 1L). In addition, immunofluorescence analysis with antibodies to CD68 revealed a dramatically increased macrophage infiltration in both the aortic wall and atherosclerotic plaques of YD mice relative to their wt controls (Figure 1M). Similarly, increased expression of activated phospho-SMAD (Figure. 1N) and increased collagen deposition (Figure 1O) were observed in the aortic sections of YD compared to wt mice, indicating increased TGF (transforming growth factor) β signaling in the aneurysms of YD mice.

No differences in systemic circulating immune cells were detected between the 2 groups (Figure 2A). However, transcriptomic characterization of the aortic tissue of wt and YD mice by quantitative PCR (Figure 2B) showed significant increase in the macrophage marker *Cd68* mRNA but no differences in *Cd4* or *Cd8* mRNA. Analysis of cytokines and inflammatory markers in the aortic tissue showed increased transmural inflammation in YD compared with wt aneurysms, including significant upregulation of *Ccl2*, *Il6*, and *Il1b*. No differences in anti-inflammatory markers *Il10*, *Arg1*, *Cd206*, and *Ym1* were observed (Figure 2C).

To delve into the molecular mechanisms underlying the pathogenic effects mediated by the MT1-MMP Y573D mutation, we analyzed the expression of Netrin-1 (*Ntn1*) in the aorta of YD and wt mice. Our rationale was based on our previous findings that this protein, a neuronal guidance cue expressed by macrophages in atherosclerotic plaques, has both proatherogenic and proaneurysmal effects.[4,21–23] As shown in Figure 2D, *Ntn1* mRNA levels were significantly increased in the aortic tissue of YD mice compared to wt controls. Immunofluorescence staining showed elevated Netrin-1 expression in both adventitial and intralesional macrophages in YD aortas, whereas in wt aortas Netrin-1 was expressed at

lower levels only by adventitial macrophages (Figure 2E). BMDM from wt mice expressed high levels of the proinflammatory markers *Il1b*, *Il6*, *Tnfa,* and *Nos2* mRNA when in M1 activated mode; however, YD BMDM showed higher levels of these cytokines (Figure 2F). *Mrc1*, the classical marker of M2 macrophages, was significantly increased in YD M2 macrophages compared to wt M2 cells. Conversely, both M1 and M2 macrophages from YD mice expressed significantly higher levels of *Ntn1* mRNA than macrophages from wt littermates (Figure 2H). Therefore, these results showed that the non-proteolytic cytoplasmic domain of MT1-MMP mediates downstream signaling that regulates the expression of Netrin-1 in aortic macrophages.

TIMP-2, a physiological inhibitor of MT1-MMP, binds with high affinity to the extracellular domain of MT1-MMP thereby inducing the activation of the Ras-ERK1/2 and AKT signaling pathways, and the MT1-MMP Y573D blocks this effect, as we previously described.[13–15] To characterize the biomolecular machinery downstream of MT1-MMP activation in macrophages, we investigated ERK1/2 activation in response to TIMP-2 stimulation in wt and YD BMDM. Consistent with previous results in fibroblasts, Western blotting and immunofluorescence analyses showed that TIMP-2 induced ERK1/2 activation in wt but not in YD BMDM (Figure 2G and 2H). Finally, we characterized the functional impact of the MT1-MMP Y573D mutation on macrophage migration. We observed that although both wt and YD BMDM migrated towards CCL2, YD macrophages displayed a reduced locomotion (Figure 2I). This is likely due to the effect of Netrin-1 acting as a migration repressor, as we have previously shown.[22] Thus, these results indicate that the pathologies observed in YD mouse aorta might be due to transmural macrophage retention within the tissue, thereby fueling inflammation.

DISCUSSION

The extracellular matrix-degrading proteinase MT1-MMP, a transmembrane protein with an extracellular proteolytic domain and a short cytoplasmic tail, is a major effector of a variety of physiological and pathological tissue remodeling processes, including vascular wall remodeling. The study of mice genetically deficient in MT1-MMP has shown that this proteinase plays opposing roles in the pathogenesis of AAA and atherosclerotic plaque.[12,24–26] MT1-MMP promotes AAA development by inducing macrophage-mediated elastolysis[11]; conversely, it limits atherogenesis by inhibiting vascular smooth muscle cell proliferation.[12] Transplantation of *Mmp14*$^{-/-}$ bone marrow into *Ldlr*$^{-/-}$ mice to isolate the contribution of myeloid-derived MT1-MMP to atherosclerosis, did not show any difference in plaque development in mice fed a high-cholesterol diet,[26] suggesting a possible compensatory mechanism from vascular smooth muscle cells. In the same study, *Mmp14*$^{-/-}$*Ldlr*$^{-/-}$ chimeras showed increased intralesional collagen accumulation, a trait associated with putative plaque stability in advanced lesions. In human studies, MT1-MMP has been shown to be associated with plaque instability in advanced atherosclerotic lesions.[24,25]

These functions of MT1-MMP have been ascribed to its proteolytic activity and show that MT1-MMP has a spatiotemporal impact on plaque development and vulnerability, likely mediated by different cellular effectors.

However, several lines of evidence have revealed proteolysis-independent, signaling functions of MT1-MMP.[13,14,27–29] The recent generation of a mouse that expresses proteolytically active MT1-MMP devoid of signaling capacity (MT1-MMP Y573D) has shown that MT1-MMP signaling controls the homeostasis of several tissues through a proteolysis-independent mechanism.[15] We used this novel mouse model to investigate the potential role of MT1-MMP signaling in the control of aortic wall homeostasis. Our analysis of AAA development using the Ang II model showed that MT1-MMP Y573D mice develop larger AAA lesions than their wt littermates, with the concomitant development of severe atherosclerotic plaques characterized by massive macrophage infiltration.

These findings reveal a thus far unknown inhibitory function of MT1-MMP in AAA development, which contrasts with the permissive role ascribed to its proteolytic activity by a previous study.[11] This seeming discrepancy can be explained by important experimental differences, and—more importantly—by considering that MT1-MMP has both proteolytic and nonproteolytic functions. The data showing that MT1-MMP promotes AAA formation were obtained using *Mmp14* knockout mice, in which both functions are abrogated. In contrast, the MT1-MMP Y573D mutation only affects the signaling function without altering the proteolytic activity of MT1-MMP,[15] and thus affords the analysis of the relative contribution of signaling to the role of MT1-MMP in tissue homeostasis. The physiological function of MT1-MMP depends on the balance of its proteolytic and nonproteolytic activities, which can be controlled by extracellular factors such as TIMP-2, whose binding to MT1-MMP blocks its proteolytic activity and, at the same time, induces activation of ERK1/2 and AKT signaling through the MT1-MMP cytoplasmic tail.[13–15]

It should also be noted that our study used a different AAA model than and the previous study with *Mmp14* knockout mice, which induced AAA formation by $CaCl_2$ application to the arterial surface.[11] The 2 experimental methods generate AAA by different mechanisms that may require different contributions of the proteolytic or signaling function of MT1-MMP. The Ang II model mimics the human pathogenetic mechanism more closely than the $CaCl_2$ method, thus implicating MT1-MMP signaling as a physiological function in the control of AAA formation and development.

Unlike our observation of increased AAA formation, our finding that MT1-MMP Y573D mice develop severe intraaneurysmal atherosclerotic lesions is consistent with the previous finding of increased atherogenesis in mice genetically deficient in MT1-MMP and ApoE, suggesting that the protective action of MT1-MMP is mediated by both its proteolytic and nonproteolytic functions.[12] It is noteworthy that, unlike in the previous study with hemizygous *Mmp14* knockout mice on an ApoE-deficient background,[12] MT1-MMP Y573D mice developed very severe atherosclerotic plaques on an $ApoE^{+/+}$ background. YD mice developed lesions after only 6 weeks of high-fat diet feeding, and we observed a high content of lipid-laden macrophages in atherosclerotic plaques. This is unlikely due to differences in plasma cholesterol levels since we observed similar cholesterol profiles between wt and YD mice at baseline and after exposure to PCSK9-AAV+Western diet and Ang II. Because we did not analyze plasma cholesterol in mice before pump implantation, we cannot exclude intermediate cholesterol fluctuations or an antecedent variability of the response to the PCSK9-AAV exposure, despite similar cholesterol levels at harvest.

We found that atherosclerotic plaque-associated, as well as BMDM of YD mice, express elevated levels of Netrin-1 relative to wt cells, a finding that can explain the high macrophage infiltrates within the atherosclerotic plaques. Previous independent work has shown that Netrin-1, a neuroimmune guidance cue secreted by macrophages in atheromas, blocks macrophage migration toward chemokines that mediate their egress from plaques,[22] and we have shown that it promotes AAA formation by upregulating MMP-3 expression in vascular smooth muscle cells.[4] The involvement of Netrin-1 is also supported by our observation of high levels of MMP-3 expression in the aortic lesions of YD mice, consistent with our previous findings.[4] Our previous work has shown that the Y573D mutation abrogates the Ras-ERK1/2 and AKT pathways triggered by TIMP-2.[13] Netrin-1 has been shown to inhibit macrophage migration through FAK (focal adhesion kinase) activation.[22] It is, therefore, foreseeable that this pathway is interconnected between the intracellular domain of MT1-MMP and the expression of Netrin-1 in aortic macrophages. Given the synchronous appearance of atherosclerotic and AAA lesions in YD mice, it is probable that the Y573D mutation engages in a signaling network that culminates in the expression of Netrin-1 in macrophages. Further studies are required to delineate these mechanisms which would further shed the light on the downstream molecular patterns regulated by the intracellular signaling of MT1-MMP.

In this study, we serendipitously observed the presence of atherosclerotic lesions in the abdominal segment of the aorta in YD mice, lesions that usually manifest in more proximal aortic segments. We, therefore, did not systematically collect data to directly investigate the temporal superposition of atherogenesis and vascular remodeling in the aneurysmal context. We do not have direct evidence of whether accelerated atherosclerosis would initially prime inflammation and vascular remodeling or vice versa. We do not report data on earlier time points in the development of combined AAA/atherosclerosis lesions. We demonstrated that TIMP-2 induced ERK1/2 phosphorylation in wt but not in YD murine BMDM. However, we did not validate this mechanism in human macrophages, and we did not assess TIMP-2–induced signaling in vivo, or in other vascular cell types. We found that YD macrophages express higher levels of Netrin-1, consistently with observed proaneurysmal and proatherogenic phenotypes from our previous studies. We acknowledge that further mechanistic validation is needed to support the direct role of Netrin-1 as one of the downstream signaling elements elicited by the activation of the intracellular domain of MT1-MMP.

CONCLUSIONS

In conclusion, our findings add a novel dimension to our understanding of the role of MT1-MMP in the concomitant AAA development and atherogenesis. MT1-MMP is a bifunctional protein with both an extracellular proteolytic and an intracellular nonproteolytic, signaling function, the concerted action of which is required for arterial wall homeostasis. This conclusion may explain the failure of synthetic inhibitors of the proteolytic activity of MMPs in the treatment of AAA,[7] and further expands our understanding on the molecular complexity of this life-threatening disease.

Supplementary Material

Refer to Web version on PubMed Central for supplementary material.

Acknowledgments

B. Ramkhelawon directed this work and cowrote the article, P. Mignatti provided mice and assisted in the in vitro experimental approach and writing of the article, M. Silvestro assisted in writing the article, performed in vitro assays, and assisted in data analysis; D. Alebrahim performed all in vivo experiments; C. Lu, C.F. Rivera, J. Vlahos, C. Tang, Z. Harpel, R. Sleiman Tellaoui, A.L. Zias, M. Silvestro, D.J. Maldonado, D. Byrd, M. Attur assisted in in vitro assays and analysis and quantification of abdominal aortic aneurysms (AAA) and lesion size. All authors approved the article and support the conclusions.

Sources of Funding

Part of this study was funded by National Institute of Health grants R01 HL146627 to B. Ramkhelawon and R01 CA136715, R01CA136715-05S1, R21 AG033735 and in part by R21 AR069240-01A1 to P. Mignatti.

Nonstandard Abbreviations and Acronyms

AAA	abdominal aortic aneurysm
AKT	serine/threonine kinase, also known as protein kinase B (PKB)
Ang II	angiotensin II
BMDM	bone marrow–derived macrophages
ERK1/2	extracellular signal-regulated kinases 1 and 2, also known as p44/42
MMP	matrix metalloproteinase
MT1-MMP	membrane-type 1 matrix metalloproteinase, also known as MMP-14
PCSK9	proprotein convertase subtilisin/kexin type 9
Ras	rat sarcoma oncogene-derived GTPase, also known as p21
TIMP	tissue inhibitor of metalloproteinases
wt	$Mmp14^{wt/wt}$
YD	$Mmp14^{Y573D/Y573D}$

REFERENCES

1. Kent KC. Clinical practice. Abdominal aortic aneurysms. N Engl J Med. 2014;371:2101–2108. doi: 10.1056/NEJMcp1401430 [PubMed: 25427112]
2. Li Y, Wang W, Li L, Khalil RA. MMPs and ADAMs/ADAMTS inhibition therapy of abdominal aortic aneurysm. Life Sci. 2020;253:117659. doi: 10.1016/j.lfs.2020.117659 [PubMed: 32283055]
3. Qian W, Hadi T, Silvestro M, Ma X, Rivera CF, Bajpai A, Li R, Zhang Z, Qu H, Tellaoui RS, et al. Microskeletal stiffness promotes aortic aneurysm by sustaining pathological vascular smooth muscle cell mechanosensation via Piezo1. Nat Commun. 2022;13:512. doi: 10.1038/s41467-021-27874-5 [PubMed: 35082286]
4. Hadi T, Boytard L, Silvestro M, Alebrahim D, Jacob S, Feinstein J, Barone K, Spiro W, Hutchison S, Simon R, et al. Macrophage-derived netrin-1 promotes abdominal aortic aneurysm formation

by activating MMP3 in vascular smooth muscle cells. Nat Commun. 2018;9:5022. doi: 10.1038/s41467-018-07495-1 [PubMed: 30479344]

5. Silvestro M, Hadi T, Cayne NS, Maldonado TS, Gelb BE, Jacobowitz GR, Ramkhelawon B. Cell-specific profiling of transcriptional landscape in human abdominal aortic aneurysm by single-cell RNA sequencing. J Vasc Surg. 2019;70:E142–E143. doi: 10.1016/j.jvs.2019.08.081
6. Rabkin SW. The role matrix metalloproteinases in the production of aortic aneurysm. Prog Mol Biol Transl Sci. 2017;147:239–265. doi: 10.1016/bs.pmbts.2017.02.002 [PubMed: 28413030]
7. Wang YD, Liu ZJ, Ren J, Xiang MX. Pharmacological therapy of abdominal aortic aneurysm: an update. Curr Vasc Pharmacol. 2018;16:114–124. doi: 10.2174/1570161115666170413145705 [PubMed: 28412911]
8. Gifford V, Itoh Y. MT1-MMP-dependent cell migration: proteolytic and non-proteolytic mechanisms. Biochem Soc Trans. 2019;47:811–826. doi: 10.1042/BST20180363 [PubMed: 31064864]
9. Itoh Y Membrane-type matrix metalloproteinases: their functions and regulations. Matrix Biol. 2015;44–46:207–223. doi: 10.1016/j.matbio.2015.03.004
10. Sato H, Takino T, Okada Y, Cao J, Shinagawa A, Yamamoto E, Seiki M. A matrix metalloproteinase expressed on the surface of invasive tumour cells. Nature. 1994;370:61–65. doi: 10.1038/370061a0 [PubMed: 8015608]
11. Xiong W, Knispel R, MacTaggart J, Greiner TC, Weiss SJ, Baxter BT. Membrane-type 1 matrix metalloproteinase regulates macrophage-dependent elastolytic activity and aneurysm formation in vivo. J Biol Chem. 2009;284:1765–1771. doi: 10.1074/jbc.M806239200 [PubMed: 19010778]
12. Barnes RH 2nd, Akama T, Öhman MK, Woo MS, Bahr J, Weiss SJ, Eitzman DT, Chun TH. Membrane-tethered metalloproteinase expressed by vascular smooth muscle cells limits the progression of proliferative atherosclerotic lesions. J Am Heart Assoc. 2017;6:e003693. doi: 10.1161/JAHA.116.003693 [PubMed: 28735290]
13. D'Alessio S, Ferrari G, Cinnante K, Scheerer W, Galloway AC, Roses DF, Rozanov DV, Remacle AG, Oh ES, Shiryaev SA, et al. Tissue inhibitor of metalloproteinases-2 binding to membrane-type 1 matrix metalloproteinase induces MAPK activation and cell growth by a non-proteolytic mechanism. J Biol Chem. 2008;283:87–99. doi: 10.1074/jbc.M705492200 [PubMed: 17991754]
14. Valacca C, Tassone E, Mignatti P. TIMP-2 interaction with MT1-MMP activates the AKT pathway and protects tumor cells from apoptosis. PLoS One. 2015;10:e0136797. doi: 10.1371/journal.pone.0136797 [PubMed: 26331622]
15. Attur M, Lu C, Zhang X, Han T, Alexandre C, Valacca C, Zheng S, Meikle S, Dabovic BB, Tassone E, et al. Membrane-type 1 matrix metalloproteinase modulates tissue homeostasis by a non-proteolytic mechanism. iScience. 2020;23:101789. doi: 10.1016/j.isci.2020.101789 [PubMed: 33294797]
16. Robinet P, Milewicz DM, Cassis LA, Leeper NJ, Lu HS, Smith JD. Consideration of sex differences in design and reporting of experimental arterial pathology studies-statement srom ATVB council. Arterioscler Thromb Vasc Biol. 2018;38:292–303. doi: 10.1161/ATVBAHA.117.309524 [PubMed: 29301789]
17. Boytard L, Hadi T, Silvestro M, Qu H, Kumpfbeck A, Sleiman R, Fils KH, Alebrahim D, Boccalatte F, Kugler M, et al. Lung-derived HMGB1 is detrimental for vascular remodeling of metabolically imbalanced arterial macrophages. Nat Commun. 2020;11:4311. doi: 10.1038/s41467-020-18088-2 [PubMed: 32855420]
18. Lu H, Howatt DA, Balakrishnan A, Graham MJ, Mullick AE, Daugherty A. Hypercholesterolemia induced by a PCSK9 gain-of-function mutation augments angiotensin II-induced abdominal aortic aneurysms in C57BL/6 mice-brief report. Arterioscler Thromb Vasc Biol. 2016;36:1753–1757. doi: 10.1161/ATVBAHA.116.307613 [PubMed: 27470509]
19. Manning MW, Cassi LA, Huang J, Szilvassy SJ, Daugherty A. Abdominal aortic aneurysms: fresh insights from a novel animal model of the disease. Vasc Med. 2002;7:45–54. doi: 10.1191/1358863×02vm413ra [PubMed: 12083734]
20. Di Lascio N, Kusmic C, Stea F, Faita F. Ultrasound-based pulse wave velocity evaluation in mice. J Vis Exp. 2017:54362. doi: 10.3791/54362 [PubMed: 28287528]

21. Alebrahim D, Nayak M, Ward A, Ursomanno P, Shams R, Corsica A, Sleiman R, Fils KH, Silvestro M, Boytard L, et al. Mapping semaphorins and netrins in the pathogenesis of human thoracic aortic aneurysms. Int J Mol Sci. 2019;20:E2100. doi: 10.3390/ijms20092100
22. van Gils JM, Derby MC, Fernandes LR, Ramkhelawon B, Ray TD, Rayner KJ, Parathath S, Distel E, Feig JL, Alvarez-Leite JI, et al. The neuroimmune guidance cue netrin-1 promotes atherosclerosis by inhibiting the emigration of macrophages from plaques. Nat Immunol. 2012;13:136–143. doi: 10.1038/ni.2205 [PubMed: 22231519]
23. Silvestro M, Hadi T, Boytard L, Alebrahim D, Jacobowitz GR, Ramkhelawon B. Macrophage-derived netrin 1 promotes abdominal aortic aneurysms by activating matrix mtalloproteinase 3 in vascular smooth muscle cells. J Vasc Surg. 2018;68:E138–E138.
24. Di Gregoli K, Jenkins N, Salter R, White S, Newby AC, Johnson JL. MicroRNA-24 regulates macrophage behavior and retards atherosclerosis. Arterioscler Thromb Vasc Biol. 2014;34:1990–2000. doi: 10.1161/ATVBAHA.114.304088 [PubMed: 24990232]
25. Johnson JL, Jenkins NP, Huang WC, Di Gregoli K, Sala-Newby GB, Scholtes VP, Moll FL, Pasterkamp G, Newby AC. Relationship of MMP-14 and TIMP-3 expression with macrophage activation and human atherosclerotic plaque vulnerability. Mediators Inflamm. 2014;2014:276457. doi: 10.1155/2014/276457 [PubMed: 25301980]
26. Schneider F, Sukhova GK, Aikawa M, Canner J, Gerdes N, Tang SM, Shi GP, Apte SS, Libby P. Matrix-metalloproteinase-14 deficiency in bone-marrow-derived cells promotes collagen accumulation in mouse atherosclerotic plaques. Circulation. 2008;117:931–939. doi: 10.1161/CIRCULATIONAHA.107.707448 [PubMed: 18250269]
27. Gonzalo P, Guadamillas MC, Hernández-Riquer MV, Pollán A, Grande-García A, Bartolomé RA, Vasanji A, Ambrogio C, Chiarle R, Teixidó J, et al. MT1-MMP is required for myeloid cell fusion via regulation of Rac1 signaling. Dev Cell. 2010;18:77–89. doi: 10.1016/j.devcel.2009.11.012 [PubMed: 20152179]
28. Sakamoto T, Seiki M. Cytoplasmic tail of MT1-MMP regulates macrophage motility independently from its protease activity. Genes Cells. 2009;14:617–626. doi: 10.1111/j.1365-2443.2009.01293.x [PubMed: 19371380]
29. Wang Y, McNiven MA. Invasive matrix degradation at focal adhesions occurs via protease recruitment by a FAK-p130Cas complex. J Cell Biol. 2012;196:375–385. doi: 10.1083/jcb.201105153 [PubMed: 22291036]

Highlights

- The proteinase MT1-MMP (matrix metalloproteinase) controls aortic wall homeostasis by a novel proteolysis-independent signaling mechanism.
- Cytoplasmic MT1-MMP signaling modulates concomitant atherosclerosis and abdominal aortic aneurysm development.
- MT1-MMP intracellular signaling might regulate macrophage expression of Netrin-1, a protein that promotes both abdominal aortic aneurysm and atherosclerotic plaque development.

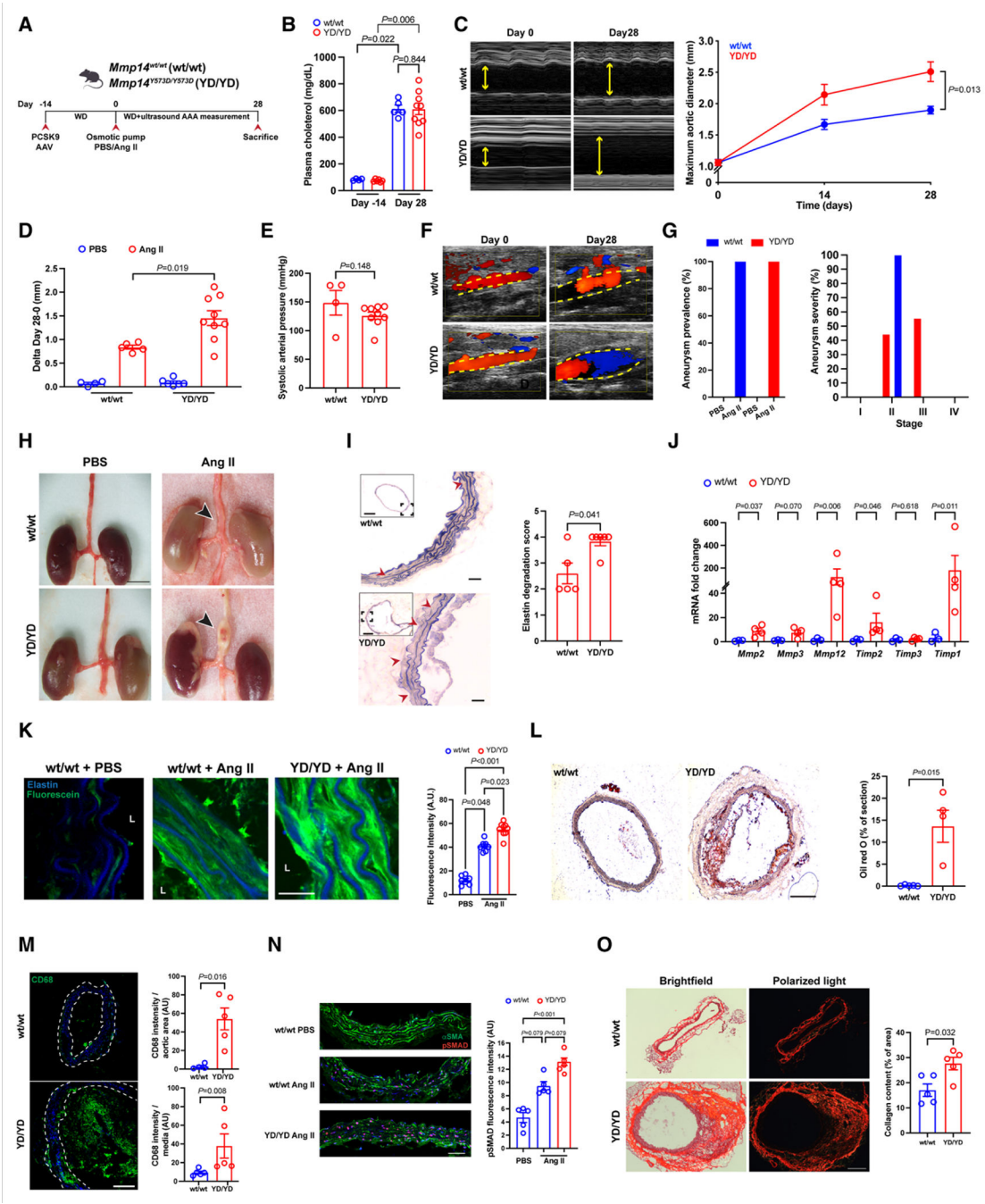

Figure 1. MT1-MMP Y573D mutation modulates abdominal aortic aneurysm and atherosclerosis.

A, Schematic outline of the experimental protocol. **B**, Plasma cholesterol levels at baseline (day –14) and harvest (day 28) in *Mmp14*$^{wt/wt}$ (wt) and *Mmp14*$^{Y573D/Y573D}$ (YD) mice as indicated. n=4–9 per group. **C**, Representative M-mode ultrasound (US) images of aortas (**left**), and diameters in Ang II (angiotensin II) infused mice (**right**), as indicated. n=5–9 per group. **D**, Pairwise difference in maximum aortic diameter between harvest and baseline (day 28–0) in PBS or Ang II–infused mice, as indicated. n=4–9 per group. **E**, Systolic

arterial pressure in Ang II–infused mice (day 28). n=4–9 per group. **F**, Representative color Doppler US images at day 0 and Day 28 as indicated. Yellow dashed line indicates the aortic wall. **G**, Prevalence (**left**) and severity (**right**) of the aneurysms, as indicated. n=4–9 per group. **H**, Representative microphotographs of aortas at euthanization as indicated. Arrowheads show aortic dilation. Scale bar: 5 mm. **I**, Representative images of Verhoeff-Van Gieson elastin staining of aortic sections (**left**) and elastin degradation score (**right**). Red arrowheads indicate elastin breaks. Scale bars: 200 μm (insert) and 50 μm. **J**, mRNA expression of indicated transcripts in abdominal aortic tissue. n=3–4 per group. **K**, Representative images of in situ zymography (fluorescein, green; **left**), and quantification (**right**) in aortic sections from wt and YD mice. Elastin autofluorescence in blue. Scale bar: 20 μm. **L**, lumen. n=7–9 per group. **L**, Representative images (**left**) and quantification (**right**) of oil red O staining in abdominal aortic sections at the level of maximum aortic diameter in mice as indicated (day 28). Scale bar: 200 μm. n=4–5 per group. **M**, Representative immunofluorescence (IF) images (**left**) and quantification (total area, **top right**; tunica media, **bottom right**) of the macrophage marker CD68 (green) in aortic sections of mice as indicated. Dashed line contours the tunica media. Scale bar: 100 μm. Nuclei in 4’,6-diamidino-2-phenylindole (DAPI; blue). n=4–5 per group. **N**, Representative IF images of αSMA (α-smooth muscle actin, green) and pSMAD (phospho-SMAD1/3/5 [mothers against decapentaplegic homolog 1/3/5], red) in the abdominal aortic wall of mice as indicated (**left**), and quantification of pSMAD (**right**). Scale bar: 50 μm. Nuclei in DAPI (blue). n=5 per group. **O**, Picrosirius red collagen staining representative images of aortic sections in Ang II–infused mice in brightfield or under polarized light as indicated (**left**), and quantification (**right**). Scale bar: 200 μm. n=5 per group. Data are presented as mean±SEM; Indicated *P* values are calculated by 2-tailed Mann-Whitney test or Kruskal-Wallis and multiple comparisons Dunn test (**B**, **D**–**O**), or by mixed-effect model (REML [restricted maximum likelihood]) with Geisser-Greenhouse correction and Sidak multiple comparisons test (**C**). AAV indicates adeno-associated viral vector; AU, arbitrary units; PCSK9, proprotein convertase subtilisin/kexin type 9; and WD, Western diet.

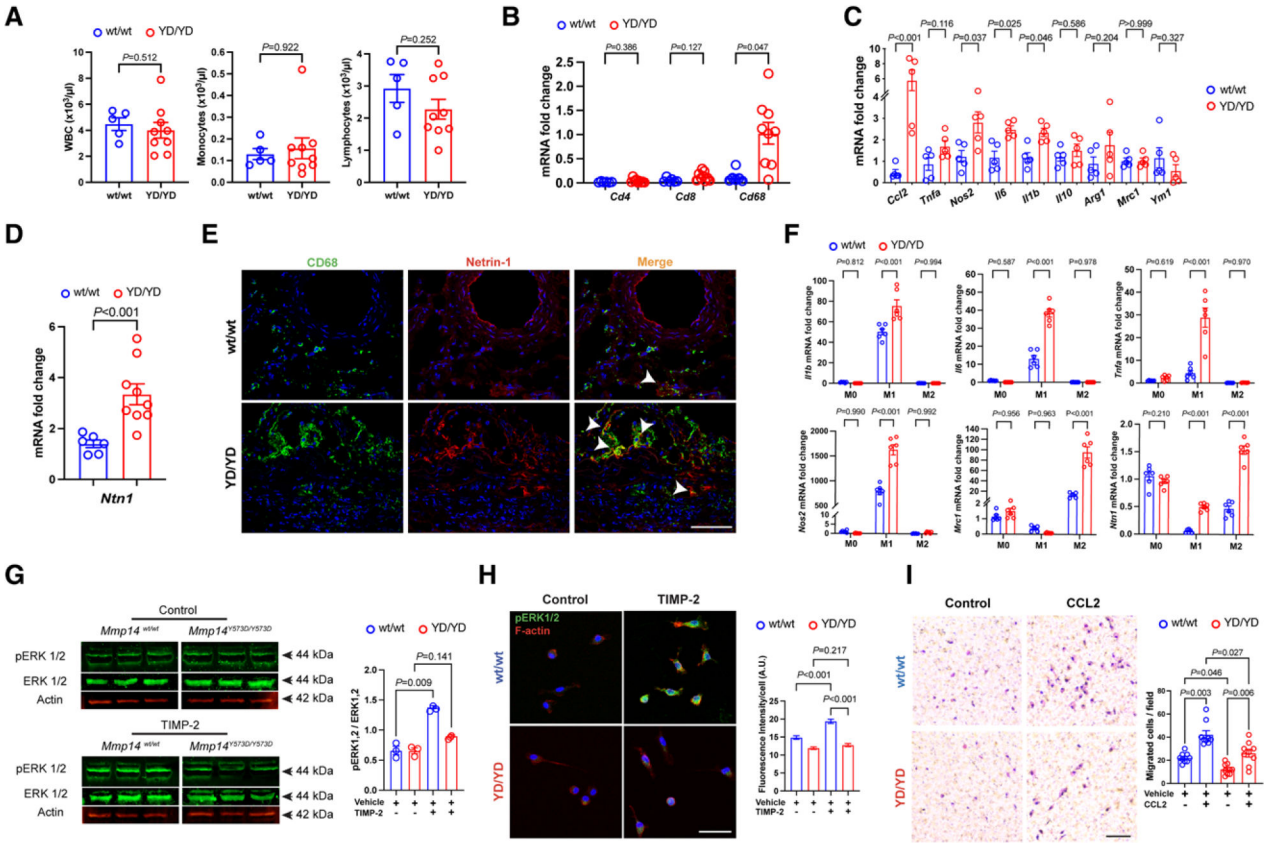

Figure 2. The intracellular domain of MT1-MMP regulates Netrin-1 in aortic macrophages to promote inflammation and migration.

A, White blood cell (WBC), monocyte, and lymphocyte count by automated blood cell count in peripheral blood of mice challenged with Ang II (angiotensin II) as indicated. n=5–9 per group. **B**–**D**, mRNA expression of indicated transcripts in the abdominal aorta of Ang II–infused mice as indicated. n=5–9 per group. **E**, Immunofluorescence (IF) staining of the macrophage marker CD68 (green) and Netrin-1 (red) in abdominal aortas of mice infused with Ang II as indicated. Arrowheads indicate colocalization of CD68 and Netrin-1. Bar scale: 100 μm. n=4 per group. **F**, Quantitative polymerase chain reaction analysis of indicated transcript abundance in polarized bone marrow–derived macrophages (BMDM) as indicated. n=6 per group. **G.** Western blotting of *Mmp14*$^{wt/wt}$ (wt) or *Mmp14*$^{Y573D/Y573D}$ (YD) BMDM stimulated with TIMP (tissue inhibitor of metalloproteinases)-2 or vehicle (control), as indicated, probed for pERK1/2 (phospho-ERK1/2 [extracellular signal-regulated kinases 1 and 2]), ERK1/2 and loading control actin (**left**). Quantification is shown in **right**. n=3 per group. **H**, Representative images (**left**) and quantification (**right**) of IF staining of pERK1/2 in wt or YD BMDM after TIMP-2 stimulation or vehicle (control), as indicated. F-actin by phalloidin staining is shown in red. Nuclei are stained with 4’,6-diamidino-2-phenylindole (blue). Scale bar: 25 μm. n=198–236 per group **I**, Representative images (**left**) and cell count of migrated cells (**right**) of wt or YD BMDM migration assay towards CCL2 (C-C motif chemokine 2) or vehicle (control) as indicated. Cells stained with Giemsa. Scale bar: 50 μm. Data are presented as mean±SEM;

Indicated *P* values are calculated by 2-tailed Mann-Whitney test or Kruskal-Wallis and multiple comparisons Dunn test.